Journal of the Ceramic Society of Japan 126 [5] 354-359 2018
DOI http://doi.org/10.2109/jcersj2.17244

JCS-Japan

FULL PAPER

Photocatalytic degradation of dyes over Au decorated $SrTiO_3$ nanoparticles under simulated sunlight and visible light irradiation

Tao XIAN[1,†], Lijing DI[1,2], Xiaofeng SUN[1], Jun MA[1], Yongjie ZHOU[1] and Xuegang WEI[1]

[1]College of Physics and Electronic Information Engineering, Qinghai Normal University, Xining 810008, People's Republic of China
[2]State Key Laboratory of Advanced Processing and Recycling of Non-ferrous Metals, Lanzhou University of Technology, Lanzhou 730050, People's Republic of China

Au–$SrTiO_3$ nanocomposites were prepared using a photocatalytic reduction method by which the Au nanoparticles with particle size of 7–26 nm were deposited on the surface of $SrTiO_3$ particles with an average diameter of ~55 nm. The structure, morphology and optical properties of products were characterized by X-ray diffraction, X-ray photoelectron spectroscopy, Transmission electron microscopy and UV–visible diffuse reflectance spectroscopy. It is found that the loaded Au nanoparticles on $SrTiO_3$ particles exist in the metallic state, and the surface plasmon resonance absorption band centered around 557 nm is obviously detected in the diffuse reflectance spectra of Au–$SrTiO_3$ nanocomposites. The photocatalytic activities of samples toward the degradation of dyes (acid orange 7 and methyl orange) were evaluated under simulated sunlight and visible light irradiation. The results indicate that the decoration of Au nanoparticles can effectively improve the photocatalytic activity of $SrTiO_3$, and the catalytic efficiency of composites is related to the content of Au. More importantly, the Au–$SrTiO_3$ nanocomposites exhibit much higher photocatalytic activity under simulated sunlight than under visible light. In addition, a possible promotion mechanism of Au nanoparticles on the photocatalytic activity of $SrTiO_3$ was proposed.

Key-words : $SrTiO_3$, Au nanoparticles, Photocatalytic activity, Dyes

[Received November 26, 2017; Accepted February 7, 2018]

1. Introduction

The dye wastewater generated from textile industry has become a serious environment pollution problem. It is reported that about 15% of world production of textile dye is directly released in the wastewater during the application processes.[1)] Most of dyes are known to be toxic and non-biodegradable under aerobic conditions. Therefore, many strategies have been proposed to eliminate the dyes in the wastewater.[1)] Among these methods, the photocatalysis has been demonstrated to be an efficient and "green" technology for the degradation of dyes and organic pollutants.[2)–5)]

As one of the important photocatalysts, perovskite strontium titanate oxide ($SrTiO_3$) exhibits pronounced photocatalytic activity for the degradation of dyes and other organics.[6)–10)] In addition, owing to its suitable conduction band (CB) and valence band (VB) position, $SrTiO_3$ has been shown to be a promising photocatalysts for the water splitting.[11)–13)] Nevertheless, bare $SrTiO_3$ can only respond to ultraviolet (UV) light (only about 5% of sunlight) due to its wide bandgap (~3.2 eV), and thus limiting its application in the photocatalysis field. To overcome this shortage, several methods have been employed to extend the light absorption range of $SrTiO_3$ to the visible region.[14)–21)] Among them, doping with other ions is a major route to narrow the bandgap of $SrTiO_3$. However, element doping may introduce recombination center of photogenerated electron–hole pairs in the semiconductor-based photocatalysts, leading to an adverse effect on the photocatalytic activity. Therefore, the development of appropriate strategy to simultaneously extend the light response range of $SrTiO_3$ and enhance its photocatalytic activity is still a challenge.

Recently, the decoration of noble metal (i.e. Ag, Au, Pt) nanoparticles on the surface of suitable photocatalysts has attracted increasing attentions as an efficient method to improve the overall photocatalytic properties of photocatalysts.[22)–24)] In the noble metal decorated photocatalysts, the noble metal nanoparticles can serve as a trap for photoinduced electrons, and therefore inhibit the recombination of photogenerated carriers.[22)] More importantly, these noble metal nanoparticles can absorb a certain range of visible light, thus inducing the surface plasmon resonance (SPR) effect.[23),24)] Under the excitation of SPR effect, the hot electrons are generated in the noble metal nanoparticles, which directly inject into the CB of the

† Corresponding author: T. Xian; E-mail: xiantao1985@126.com

attached photocatalysts. These hot electrons and holes remaining in the noble metal nanoparticles can participate in the photocatalytic reaction, thus making photocatalysts possess visible light photocatalytic activity. Moreover, this SPR effect can enhance the local electric field of neighboring semiconductors, leading to an increase of photogenerated electron–hole separation rate.

Up to now, Au-decorated $SrTiO_3$ has been found to exhibit enhanced visible light photocatalytic activity for iso-propanol and NO degradation, water splitting and syngas production.[18)–21)] However, there is little work report on the visible light photocatalytic activity of Au-decorated $SrTiO_3$ for dye degradation. Furthermore, in the view of practical application, it is expected that the photocatalysts should exhibit efficient sunlight photocatalytic activity. Unfortunately, the photocatalytic performance and mechanism of Au-decorated $SrTiO_3$ under sunlight irradiation is rarely investigated. In this work, the Au nanoparticles decorated $SrTiO_3$ photocatalysts were fabricated by a photocatalytic reduction method. The photocatalytic activities of Au–$SrTiO_3$ nanocomposites were evaluated by the degradation of dyes under visible light and simulated sunlight irradiation. The photocatalytic mechanism of Au–$SrTiO_3$ was discussed in detail.

2. Experimental

The $SrTiO_3$ nanoparticles were synthesized by a polyacrylamide gel route as previously reported.[25)] Deposition of Au nanoparticles onto the $SrTiO_3$ surface was performed through the following procedure. 0.1 g of $SrTiO_3$ and 0.025 g of ammonium oxalate were added into 50 ml distilled water under magnetic stirring to obtain a homogeneous suspension. Then a certain volume of $HAuCl_4$ solution (0.02 M) was added to the mixture following by stirring for several minutes. Subsequently, the suspension was irradiated by low-pressure mercury lamp for 30 min and continuously bubbled with argon gas. During the reaction process, a color change from white to purple was gradually observed, suggesting the reduction of Au^{3+} to Au nanoparticles on the $SrTiO_3$ surface. Finally, the precipitate were collected by centrifugation and washed with distilled water and ethanol for several times, and then dried at 60°C for 8 h in a vacuum thermostat drier. To investigate the effect of the Au content on the photocatalytic activity of Au–$SrTiO_3$ nanocomposites, a series of samples were prepared with different $HAuCl_4$ solution volume of 0.2, 0.5, 0.8, 1.1 and 1.4 mL, and named as samples 0.2Au–$SrTiO_3$, 0.5Au–$SrTiO_3$, 0.8Au–$SrTiO_3$, 1.1Au–$SrTiO_3$ and 1.4Au–$SrTiO_3$, respectively.

Acid orange 7 (AO7) and methyl orange (MO) were used as the target pollution to examine the photocatalytic activity of the samples. A 200 W xenon lamp was employed as the simulated sunlight source. In the case of visible light reaction, a 420 nm cutoff filter was utilized to remove UV light. In a typical experimental, 0.1 g sample was dispersed in 200 ml (10 mg/L) dye aqueous solution. Prior to reaction, this suspension was magnetically stirred in dark for 0.5 h to ensure an adsorption–desorption equilibrium of dye molecule on the photocatalysts surface. During the degradation process, about 3 ml of reaction solution was collected at regular intervals of 1.5 h and centrifuged to separate the photocatalysts. The dye concentration was measured by detecting the absorbance of the supernatant at the fixed wavelength ($\lambda_{AO7} = 484$ nm and $\lambda_{MO} = 464$ nm) using an UV–visible spectrophotometer.

The electrochemical impedance spectra (EIS) of samples were performed on the electrochemical workstation (CST 350) with a three-electrode cell. In this three-electrode system, a platinum foil and a standard calomel electrode were employed as the counter and reference electrode, respectively. The working electrode was fabricated as follows: 15 mg photocatalysts, 0.75 mg carbon black and 0.75 mg polyvinylidene fluoride (PVDF) were added into 1-methyl-2-pyrrolidione (NMP) to produce slurry, and then uniformly coated on a $1.0 \times 1.0\,cm^2$ fluoride-doped tin oxide (FTO) glass electrode. After that, the electrode was dried at 60°C for 5 h. A 200 W Xe lamp was used as the light source. The photoelectrochemical measurement was carried out in the 0.1 M Na_2SO_4 electrolyte solution. The EIS plots were tested at alternating current (AC) voltage with amplitude of 5 mV and in the frequency range from 10^{-2} to 10^5 Hz.

The phase purity and crystallinity of the products were examined by X-ray diffractometer (XRD). The morphology and structure of the samples were observed by transmission electron microscope (TEM) and high-resolution TEM (HRTEM). The elemental composition of products was detected by energy-dispersive X-ray spectroscope (EDX) attached on TEM. The chemical status of Au element in the nanocomposites was investigated through the X-ray photoelectron spectroscope (XPS). The UV–visible spectrophotometer was used to record the UV–visible diffuse reflectance spectra (DRS) of samples.

3. Results and discussion

Figure 1 shows XRD diffraction patterns of $SrTiO_3$ and Au–$SrTiO_3$ samples. It can be seen that the major diffraction peaks of the samples can be indexed to cubic structure of $SrTiO_3$, which matched well with the standard XRD

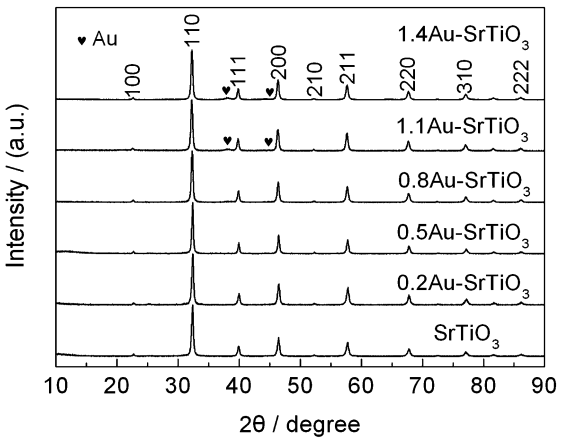

Fig. 1. XRD patterns of $SrTiO_3$ and Au–$SrTiO_3$ samples.

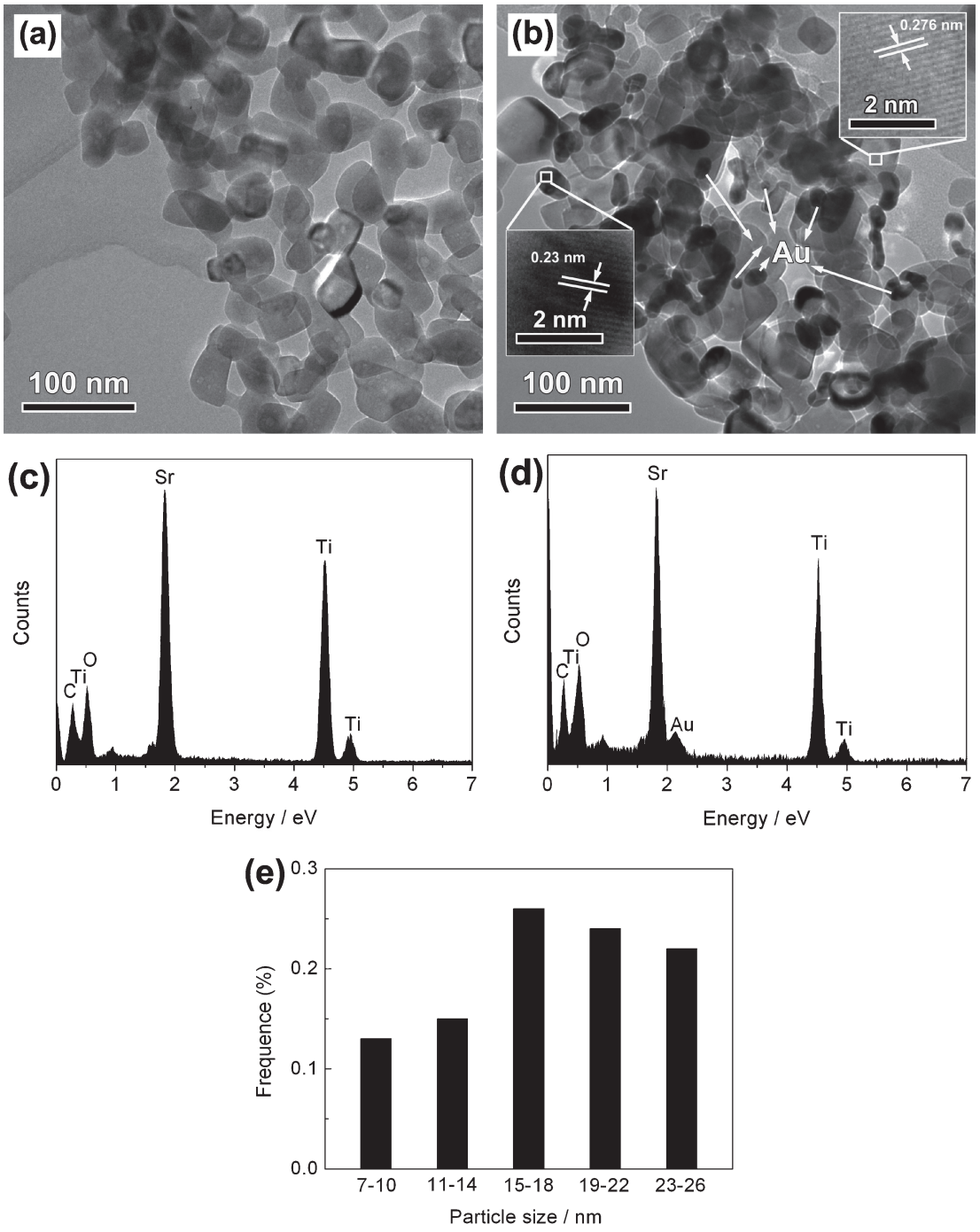

Fig. 2. (a) TEM image of $SrTiO_3$; (b) TEM image of 0.8Au–$SrTiO_3$, inset shows HRTEM of 0.8Au–$SrTiO_3$; (c) and (d) EDX spectra of $SrTiO_3$ and 0.8Au–$SrTiO_3$, respectively; (e) Particle size distribution of Au nanoparticles taken from Fig. 2(b).

data (PDF 89-4934). Notably, the diffraction peaks of $SrTiO_3$ phase in nanocomposites did not show detectable shift compared with bare $SrTiO_3$, suggesting the good structural stability of $SrTiO_3$ under the photocatalytic reduction condition. Moreover, for the 1.1Au–$SrTiO_3$ and 1.4Au–$SrTiO_3$ samples, weak diffraction peaks belonging to Au can be detected. While no obvious diffraction peaks of Au is observed in the other nanocomposites. This behavior is mainly attributed to the relatively low content of Au.

Figures 2(a) and 2(b) present the TEM images of $SrTiO_3$ and 0.8Au–$SrTiO_3$ samples, respectively. As can be seen, $SrTiO_3$ nanoparticles exhibit irregular sphere-like shape with smooth surface and its average particle size is centered around 55 nm [Fig. 2(a)]. From Fig. 2(b), one can see that small nanoparticles are well deposited on the surface of $SrTiO_3$. In the inset of Fig. 2(b), the HRTEM images taken from selected regions obviously indicate two distinct sets of lattice fringes, the interplanar distance of 0.23 and 0.276 nm corresponds well to the Au (111) and

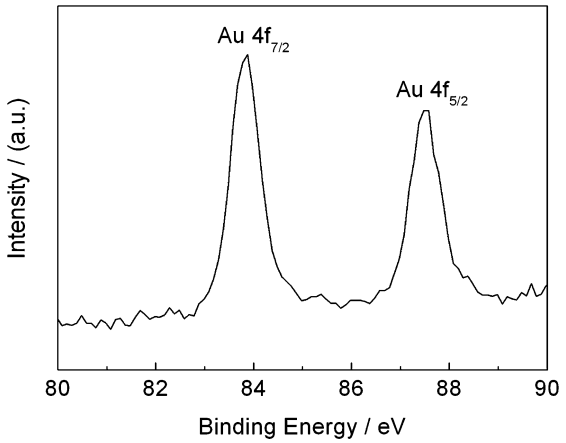

Fig. 3. High-resolution XPS spectrum of Au 4f in 0.8Au–$SrTiO_3$ sample.

$SrTiO_3$ (110) planes, respectively. The EDX analysis exhibits that $SrTiO_3$ particles include Sr, Ti and O elements [Fig. 2(c)]. Beside these elements, the EDX analysis of 0.8Au–$SrTiO_3$ confirms the presence of Au element [Fig. 2(d)]. All of the above results demonstrate that Au nanoparticles are successfully decorated onto the surface of $SrTiO_3$ particles. Additionally, the size distribution of Au nanoparticles taken from Fig. 2(b) is presented in Fig. 2(e), these gold nanoparticles exhibit a wide distribution of diameters ranging from 7 to 26 nm.

To determine the chemical status of Au element on the surface of 0.8Au–$SrTiO_3$, the XPS characterization was performed. As shown in **Fig. 3**, the high-resolution XPS spectrum of Au 4f consists of two peaks at the binding energies of 83.8 and 87.5 eV, ascribed to Au^0 $4f_{7/2}$ and Au^0 $4f_{5/2}$, respectively.[26] Furthermore, no shoulder peak for Au oxidation state is observed. The result suggests that the loaded Au nanoparticles on the $SrTiO_3$ exist in its metallic form.[26]

To investigate the optical properties of $SrTiO_3$ and Au–$SrTiO_3$ samples, the UV–visible diffuse reflectance spectra of samples are recorded and shown in **Fig. 4**(a), and their corresponding first derivative of the reflectance (R) with respect to wavelength λ (i.e. $dR/d\lambda$) are presented in Fig. 4(b). Generally, the peak wavelength in the derivative spectrum corresponds to the absorption edge of sample. From Fig. 4(a), it is clear that a broad absorption band centered at 557 nm is found in the Au–$SrTiO_3$ samples compared with pure $SrTiO_3$, which is caused by the SPR of Au nanoparticles.[23] One can see from Fig. 4(b) that all the samples exhibit a similar absorption edge at ~370 nm. This is attributed to the intrinsic bandgap absorption of $SrTiO_3$.[25] Based on the above absorption edges, the bandgap of samples can be calculated to be ~3.35 eV. It is worth noting that $SrTiO_3$ undergoes no obvious bandgap change in the nanocomposites, which is ascribed to the fact that the surface modification with small amount of Au nanoparticles cannot significantly change the energy band structure of $SrTiO_3$.

Figure 5 shows the profiles of the AO7 degradation precentage versus exposure time over obtained samples

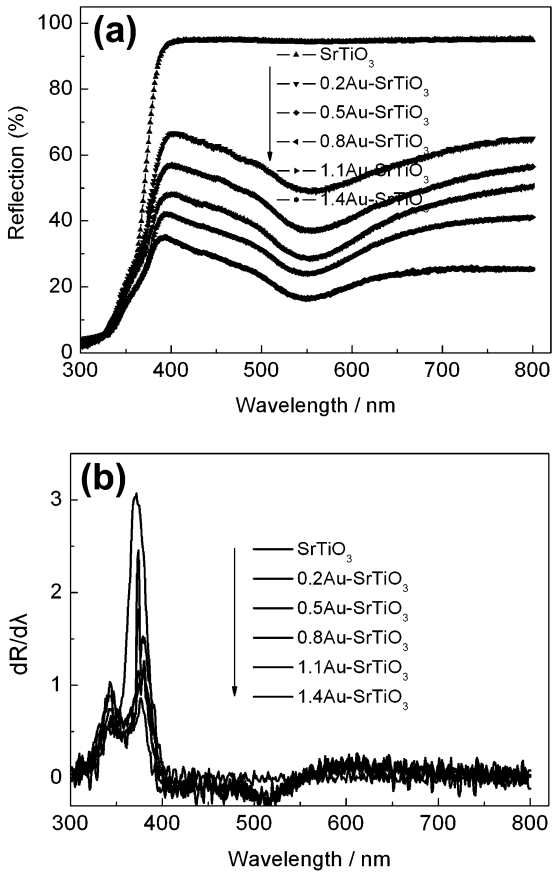

Fig. 4. (a) UV–visible diffuse reflectance spectra of the $SrTiO_3$ and Au–$SrTiO_3$ samples, (b) the corresponding first derivative of the diffuse reflectance spectra.

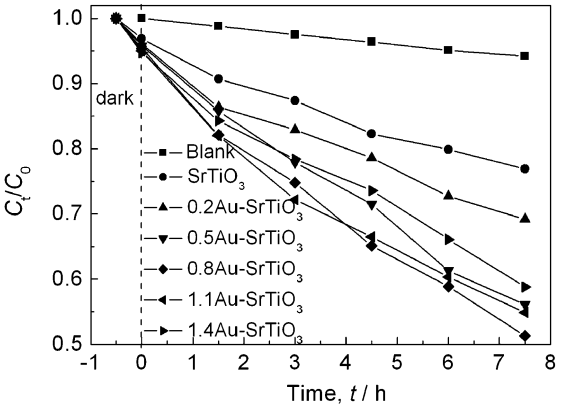

Fig. 5. Photocatalytic degradation of AO7 as a function of visible light irradiation time without catalyst and in the presence of $SrTiO_3$ and Au–$SrTiO_3$ samples.

under visible light irradiation. The blank experiment reveals that the self-degradation of AO7 is less than ~6% without catalyst after 7.5 h irradiation, suggesting the good stability of AO7 under visible light illumination. The photocatalytic results indicate that pure $SrTiO_3$ possesses weak photocatalytic activity. After the decoration of Au nanoparticles, the photocatalytic efficiency of Au–$SrTiO_3$ samples can be enhanced as compared to that of $SrTiO_3$ nanoparticles. It is worth noting that with the increase of Au content, the photocatalytic efficiency of composites

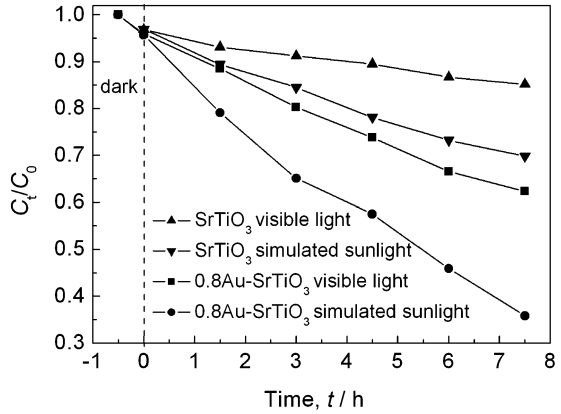

Fig. 6. Photocatalytic degradation of MO over $SrTiO_3$ and 0.8Au–$SrTiO_3$ sample with reaction time under visible light and simulated sunlight illumination.

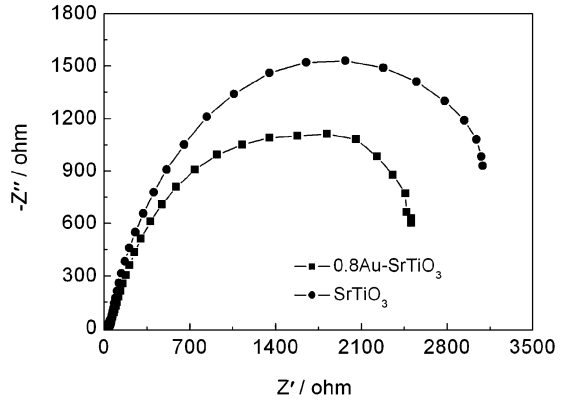

Fig. 7. The EIS spectra of $SrTiO_3$ and 0.8Au–$SrTiO_3$ samples.

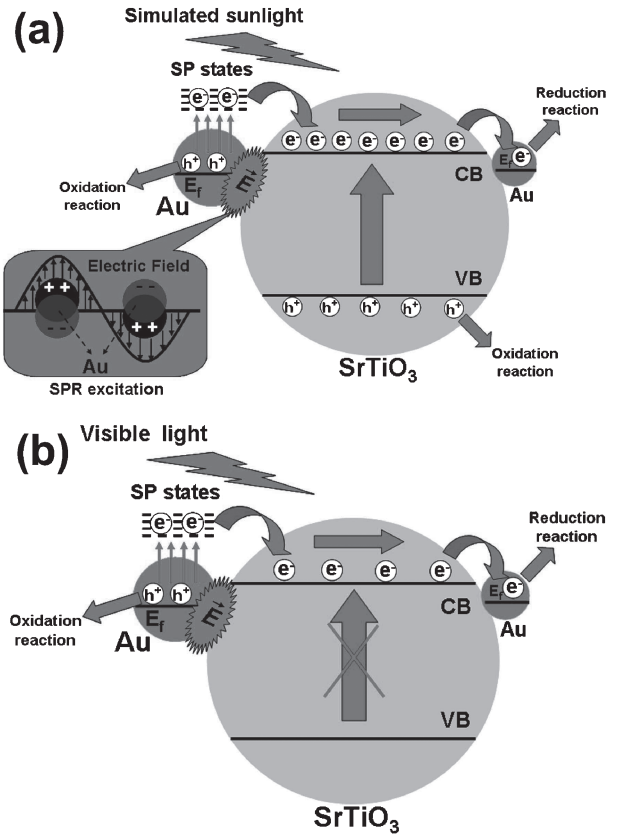

Fig. 8. Schematic of the proposed photocatalytic mechanism for dye degradation over Au–$SrTiO_3$ sample (a) under simulated sunlight irradiation and (b) under visible light irradiation.

enhances gradually. The highest photocatalytic activity is observed for 0.8Au–$SrTiO_3$ sample. However, further increase of Au content results in a decrease of photocatalytic activity. A possible reason for the reduction of the catalytic efficiency is that excessive amount of Au nanoparticles becomes the recombination center for photogenerated charges.

The photocatalytic activity of 0.8Au–$SrTiO_3$ was also evaluated by the degradation of MO under visible light and simulated sunlight irradiation, as shown in **Fig. 6**. $SrTiO_3$ can decompose only about 31% of MO after 7.5 h simulated sunlight illumination. In comparison, 0.8Au–$SrTiO_3$ exhibits remarkable enhanced simulated sunlight photocatalytic degradation efficiency. Noticeably, it is found that the simulated sunlight catalytic activity of 0.8Au–$SrTiO_3$ is superior to its visible light catalytic activity.

To understand the behavior of photogenerated charges, the electrochemical impedance spectra (EIS) of $SrTiO_3$ and 0.8Au–$SrTiO_3$ samples were performed, as shown in **Fig. 7**. It can be seen that the arc radius on the EIS curve of 0.8Au–$SrTiO_3$ is smaller than that of $SrTiO_3$, indicating the relatively lower charge-transfer resistance for the composite. This suggests that the decoration of Au nanoperticles on $SrTiO_3$ can promote separation of photogenerated electron–hole pairs and interfacial charges migration and thus leading to an increased availability of photogenerated charges for the photocatalytic reaction.

Figures 8(a) and 8(b) presents possible photocatalytic mechanism of Au–$SrTiO_3$ for dye degradation under simulated sunlight and visible light illumination, respectively. Under simulated sunlight irradiation, VB electrons are excited to the CB of $SrTiO_3$, thus creating photoinduced electron–hole pairs. Meanwhile, the larger Au particles can absorb a certain range of visible light to induce the SPR effect.[27] During this process, the electrons near the Fermi level of Au can be excited to surface plasmon (SP) states.[23] The potential of SP states is negative to the CB potential of $SrTiO_3$, so these excited electrons (hot electrons) will be injected into the CB of $SrTiO_3$, and the leaving holes on the surface of Au nanoparticles can achieve oxidize reaction. Moreover, the SPR effect is able to enhance the localized electric field near the interface of Au–$SrTiO_3$.[23] This SPR-enhanced localized electric field promotes the separation of photogenerated electron–hole pairs in the $SrTiO_3$. On the other hand, it is known that the smaller Au nanoparticles often act as electron accepter to capture the photoexcited electrons,[27] and the enhanced separation of photogenerated charges in the Au-decorated $SrTiO_3$ photoatalysts is confirmed by EIS spectra (see Fig. 7). The Fermi level of Au is positive to the CB potential of $SrTiO_3$, revealing that the photogenerated electrons on the CB of $SrTiO_3$ can readily transfer into

smaller Au nanoparticles. Such a charge migration process further suppresses the recombination of photogenerated electron–hole pairs. As a result, based on the above synergetic promotion effect of Au nanoparticles, the photogenerated charges of $SrTiO_3$ and Au nanoparticles are increasingly available to take part in the catalytic reaction, leading to the enhancement of photocatalytic activity.

As shown in Fig. 8(b), upon irradiation with visible light, the photoinduced charges are not able to generate in the $SrTiO_3$. In contrast, the Au nanoparticles can be excited by the SPR effect, and the hot electrons migration of the excited Au nanoparticles is similar to that of simulated sunlight illuminated Au–$SrTiO_3$ [Fig. 8(a)]. It is clear that photogenerated charges yield under visible light irradiation is lower than that under simulated sunlight illumination. This is why Au–$SrTiO_3$ exhibits relatively weak visible light photocatalytic activity.

4. Conclusions

In summary, the Au nanoparticles were successfully deposited on the surface of $SrTiO_3$ particles by a simple photocatalytic reduction method. The SPR effect of Au nanoparticles endows the Au–$SrTiO_3$ nanocomposites with obvious light absorption entered around 557 nm. The photocatalytic degradation of dyes under irradiation of visible light and simulated sunlight demonstrates an obvious enhancement of the catalytic activity of $SrTiO_3$ after the decoration of Au nanoparticles. This behavior is mainly attributed to the following reasons: (i) the Au nanoparticles can be excited by a certain range of visible light to induce the SPR effect; (ii) this SPR effect offers more photogenerated charges for the catalytic reaction, and furthermore SPR-enhanced localized electric field promotes the photoinduced electron–hole pair separation in the $SrTiO_3$; (iii) the photogenerated electrons of $SrTiO_3$ will transfer to the Au nanoparticles, leading to the inhibition of the photoinduced electron–hole pair recombination. In addition, it is worth noting that the Au–$SrTiO_3$ exhibits improved simulated sunlight photocatalytic activity compared to its visible light photocatalytic activity. This can be explained by the fact that the photogenerated charges yield of nanocomposites under simulated sunlight irradiation is higher than that under visible light illumination.

Acknowledgments This work was supported by the National Natural Science Foundation of China (Grant No. 51602170), the Natural Science Foundation of Qinghai, China (Grant No.2016-ZJ-954Q, 2016-ZJ-915), "ChunHui" Program of Ministry of Education of China (Grant No. Z2016074, Z2016075) and the Youth Science Foundation of Qinghai Normal University (15ZR07). 2016 Qinghai Undergraduate Training Programs for Innovation and Entrepreneurship.

References

1) O. J. Hao, H. Kim and P. C. Chiang, *Crit. Rev. Env. Sci. Tec.*, 30, 449–505 (2000).
2) L. Di, H. Yang, T. Xian and X. Chen, *Materials*, 10, 1118 (2017).
3) F. Wang, H. Yang and Y. Zhang, *Mat. Sci. Semicon. Proc.*, 73, 58–66 (2018).
4) S. Zeng, J. Yang, X. Y. Qiu, Z. Y. Liang and Y. M. Zhang, *J. Ceram. Soc. Jpn.*, 124, 1152–1156 (2016).
5) H. Zou, J. Ren, X. Wu, Y. Dai, D. W. Sha, Y. Z. Wu, J. M. Pan, X. M. Lv, H. Tang and X. H. Yan, *J. Ceram. Soc. Jpn.*, 124, 1046–1051 (2016).
6) Y. S. Zhu, P. A. Salvador and G. S. Rohrer, *Phys. Chem. Chem. Phys.*, 19, 7910–7918 (2017).
7) J. F. Cao, X. S. Huang, Y. Liu, J. G. Wu and Y. X. Ji, *Mater. Res. Express*, 3, 115903 (2016).
8) L. F. da Silva, O. F. Lopes, V. R. de Mendonca, K. T. G. Carvalho, E. Longo, C. Ribeiro and V. R. Mastelaro, *Photochem. Photobiol.*, 9, 371–378 (2016).
9) S. X. Ouyang, P. Li, H. Xu, H. Tong, L. Q. Liu and J. H. Ye, *ACS Appl. Mater. Interfaces*, 6, 22726–22732 (2014).
10) T. Xian, H. Yang, J. F. Dai, Z. Q. Wei, J. Y. Ma and W. J. Feng, *Mater. Lett.*, 65, 3254–3257 (2011).
11) K. Yu, C. X. Zhang, Y. Chang, Y. J. Feng, Z. Q. Yang, T. Yang, L. L. Lou and S. X. Liu, *Appl. Catal. B-Environm*, 200, 514–520 (2017).
12) A. L. Sangle, S. Singh, J. Jian, S. R. Bajpe, H. Y. Wang, N. Khare and J. L. MacManus-Driscoll, *Nano Lett.*, 16, 7338–7345 (2016).
13) B. Wang, S. H. Shen and L. J. Guo, *ChemCatChem*, 8, 798–840 (2016).
14) C. B. Liu, G. L. Wu, J. B. Chen, K. Huang and W. D. Shi, *New J. Chem.*, 40, 5198–5208 (2016).
15) G. J. Xing, L. X. Zhao, T. Sun, Y. G. Su and X. J. Wang, *Springerplus*, 5, 1132 (2016).
16) H. W. Kang and S. B. Park, *Int. J. Hydrogen Energ.*, 41, 13970–13978 (2016).
17) W. L. Zhao, W. Zhao, G. Zhu, T. Lin, F. Xu and F. Huang, *CrystEngComm*, 17, 7528–7534 (2015).
18) H. Liu, T. Wang, H. Zhang, G. Liu, P. Li, L. Liu, D. Hao, J. Ren, K. Chang, X. Meng, H. Wang and J. Ye, *J. Mater. Chem. A*, 4, 1941–1946 (2016).
19) D. Li, S. Ouyang, H. Xu, D. Lu, M. Zhao, X. Zhang and J. Ye, *Chem. Commun.*, 52, 5989–5992 (2016).
20) L. Liu, P. Li, B. Adisak, S. Ouyang, N. Umezawa, J. Ye, R. Kodiyath, T. Tanabe, G. V. Ramesh, S. Ueda and H. Abe, *J. Mater. Chem. A*, 2, 9875–9882 (2014).
21) T. Puangpetch, S. Chavadej and T. Sreethawong, *Energ. Convers. Manage.*, 5, 2256–2261 (2011).
22) T. Xian, H. Yang, L. J. Di and J. F. Dai, *Phys. Scripta*, 90, 2463–2469 (2015).
23) N. Zhou, V. Lopez-Puente, Q. Wang, L. Polavarapu, I. Pastoriza-Santos and Q. H. Xu, *RSC Adv.*, 5, 29076–29097 (2015).
24) P. Wang, B. Huang, Y. Dai and M. H. Whangbo, *Phys. Chem. Chem. Phys.*, 14, 9813–9825 (2012).
25) T. Xian, H. Yang, J. F. Dai, Z. Q. Wei, J. Y. Ma and W. J. Feng, *Mater. Lett.*, 65, 3254–3257 (2011).
26) X. Ke, X. Zhang, J. Zhao, S. Sarina, J. Barry and H. Zhu, *Green Chem.*, 15, 236–244 (2013).
27) J. Yan, G. Wu, N. Guan and L. Li, *Chem. Commun.*, 49, 11767–11769 (2013).